Dalton Transactions

Accepted Manuscript

ROYAL SOCIETY OF CHEMISTRY

www.rsc.org/dalton

N,N'-bis((6-methoxylpyridin-2-yl)methylene)-*p*-phenylenediimine based d^{10} transition metal complexes and their utilization in co-sensitized solar cells

Liguo Wei,[a,b] Yulin Yang,*[a] Ruiqing Fan,*[a] Yong Na,[a] Ping Wang,[a] Yuwei Dong,[a] Bin Yang,[a] Wenwu Cao[a,c]

[a] *Department of Chemistry, Harbin Institute of Technology, Harbin 150001, P.R. China*

[b] *Modern Analysis and Research Center, Heilongjiang University of Science and Technology, Harbin 150027, P.R. China*

[c] *Materials Research Institute, The Pennsylvania State University, Pennsylvania 16802, USA*

To whom the correspondence should be addressed.

Prof. Yulin Yang and Ruiqing Fan

Department of Chemistry

Harbin Institute of Technology, Harbin 150001, P. R. China

Fax: +86-451-86418270

E-mail: ylyang@hit.edu.cn and fanruiqing@hit.edu.cn

N,N'-bis((6-methoxylpyridin-2-yl)methylene)-*p*-phenylenediimine based four-coordinated d^{10} transition metal complexes (named ML, M = Zn, Cd, Hg) were synthesized and employed as co-sensitizers and co-adsorbents in combination with a ruthenium complex N719 in dye sensitized solar cells. After co-sensitization, not only the incident-photon-to-current conversion efficiency is enhanced but also the dark current is reduced. A short circuit current density of 14.46 mA cm^{-2}, an open circuit voltage of 0.74 V and a fill factor of 0.62 corresponding to an overall conversion efficiency of 6.65% under AM 1.5G solar irradiation were achieved when ZnL was used as co-sensitizer, which is much higher than that for DSSCs only sensitized by N719 (5.22%) under the same condition. The improvement in efficiency is attributed to the fact that N,N'-bis((6-methoxylpyridin-2-yl)methylene)-*p*-phenylenediimine coordinated complexes overcome the deficiency of N719 absorption in the low wavelength region of visible spectrum, prevent its aggregation, offset competitive visible light absorption of I_3^- and reduce charge recombination due to formation of a effective cover layer of the dye molecules on the TiO_2 surface. As a result, the synthesized complexes are promising candidates as co-adsorbents and co-sensitizers for highly efficient DSSCs.

1. Introduction

Since O'Regan and Grätzel first reported dye sensitized solar cells (DSSCs) in 1991, DSSCs have drawn the attention of many researchers due to their ability of converting sunlight to electricity at moderate efficiencies with low cost fabrication technique compared with conventional silicon solar cells.[1-3] However, much improvement in efficiency is desired for these devices before they could take place of the Si based solar cells. Recently, several strategies have been utilized to improve the photovoltaic performance of DSSCs, among which co-sensitization is an effective approach to enhance the device performance through a combination of two or more dyes sensitized on a same semiconductor film together, extending the light-harvesting spectrum so as to increase the photocurrents of the devices. For example, the record high performance (12.3%) of co-sensitized DSSCs was reported by Grätzel et al. using a metal-containing porphyrin dye (YD2-o-C8) and a organic dye (Y123) together with a Co(II/III)-based redox electrolyte.[4] Nazeeruddin et al. employed different NIR dyes (TT1 and SQ1) as the co-sensitizers of JK2,[5,6] and an efficiency of over 7% was achieved. Chen and Dehghani co-sensitized porphyrin dye with others respectively, resulting in enhanced efficiency which was higher than individual dye sensitized solar cells.[7,8] Co-sensitization of TiO_2 films with black dye and organic dyes(D131 or Y1) significantly enhanced photocurrent and the device performance attained η = 11.0~11.1%.[9-12] Ruthenium dye such as N719 co-sensitized with organic dyes also obtained enhanced devices performance than single N719 sensitized solar cells.[13-15] And co-sensitization of two metal-free organic sensitizers has also achieved a higher efficiency than single dye sensitized DSSCs.[16-18] Most of these works mainly concentrated on the selection of sensitizer combinations aiming at maximizing spectral compensation, which is an effective approach to enhance the light-harvesting property of DSSCs. However, the competitive light absorption of triiodide,[19,20] aggregation of dyes[21-23] and recombination of charge[24] are also the main factors to affect the performance of DSSCs.[25] Therefore, synthesis of a co-sensitizer or co-adsorbent, which could not only compensate the absorption spectra but also overcome the competitive light absorption by I^-/I_3^-, avoid dye aggregation and reduce charge recombination, is meaningful to enhance the performance of DSSCs by co-sensitization.

In the previous work of our group, metal-organic complexes including d^{10} transition

metal complexes were introduced to DSSCs system as co-sensitizers.[26-28] It has been found that d^{10} transition metal complexes with pyridine-type ligands lead to a significant increase in overall conversion efficiency of DSSCs by co-sensitization with N719. In this work, in order to overcome the competitive light absorption by I^-/I_3^- in the DSSCs system sensitized by N719, another pyridine-containing ligand N,N'-bis((6-methoxylpyridin-2-yl)methylene)-*p*-phenylenediimine is selected to synthesize a series of new d^{10} transition metal complexes (ML, M=Zn, Cd, Hg) as co-sensitizers of N719, respectively. All of these co-sensitized devices exhibited enhancements of photovoltaic performance both in J_{sc} and V_{oc}. The prepared complexes can be used as co-sensitizers and co-adsorbents to absorb light in the low wavelength region of the visible spectrum, overcome the competitive light absorption by I^-/I_3^-, avoid dye aggregation and reduce charge recombination. These synthesized Zn(II), Cd(II) and Hg(II) d^{10} transition metal complexes do help to improve the devices performance.

2. Experimental section

2.1 The synthesis of ZnL, CdL and HgL

All reagents were commercially available and used with further purification. The N,N'-bis((6-methoxylpyridin-2-yl)methylene)-*p*-phenylenediimine based d^{10} transition metal complex of ZnL was synthesized according to the following method: 6-Methoxypyridine-2-carbaldehyde (40 mmol, 3.80 mL) was added to a mixture of 1,4-Phenylenediimine (20 mmol, 2.16 g) and ethanol (70 mL). The mixture was heated and refluxed for 6 h, then cooled down and the yellow powder of N,N'-bis((6-methoxylpyridin-2-yl)methylene)-*p*-phenylenediimine was filtrated out, washed with ether and recrystallized with hexane. Then the obtained yellow needle like crystal sample (0.1 mmol, 0.0358 g) was dissolved in 25 ml of CH_2Cl_2 and a solution of zinc chloride (0.2 mmol, 0.0272 g of $ZnCl_2$ in 10 mL of methanol) was added under room temperature and then heated and refluxed for 6 h. After cooling and removal of the solvent, the residue was dissolved with acetonitrile (30 ml) and refluxed for another 3 h under 85 ºC, then filtered into a beakerflask, volatilized for about 6 h, a desired rhombus crystal was obtained.

$C_{15}H_{19}N_3OZnCl_2$, Yield: 75%, UV-vis (nm, in ethanol, 25 ºC): 213, 246, 287, 365, 500.

^{1}H NMR (400 MHz, DMSO-d_6): δ = 8.49 (s, 1H, C*H*=N), 7.81 (t, 1H, Py-H_4), 7.70 (d, 1H, Py-H_3). 7.23 (d, 2H, *o*-Ph), 6.89 (d, 1H, Py-H_5), 6.63 (d, 2H, *m*-Ph), 5.42 (s, 2H, NH_2), 3.94 (s, 3H, OCH_3). FT-IR (KBr, cm^{-1}): 3429 (w, ν_{N-H}), 1630 (m, $\nu_{C=N}$), 1599 (s), 1550 (s), 1479 (s), 1374 (m), 1291 (s), 1171 (s), 1098 (m), 1016 (m), 960 (m), 830 (m), 797 (m), 512 (m). Element analysis for $C_{15}H_{19}N_3OZnCl_2$ (M_r: 365.56): Calcd: C, 42.71%; H, 3.58%; N, 11.49%. Found: C, 42.55%; H, 3.72%; N, 11.39%.

The synthesis procedure of CdL and HgL were the same as that for ZnL except that $ZnCl_2$ was replaced by $CdCl_2$ (0.2 mmol, 0.0456 g) and $HgCl_2$ (0.2 mmol, 0.0544 g), respectively. The synthesis of complexes ZnL, CdL and HgL are summarized in Scheme 1.

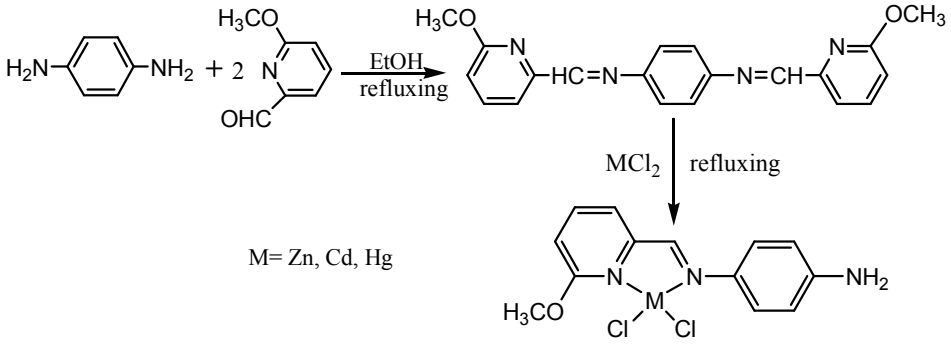

Scheme 1 Synthesis routes of ZnL, CdL and HgL.

$C_{15}H_{19}N_3OCdCl_2$, Yield: 78%, UV-vis (nm, in ethanol, 25 ºC): 217, 246, 304, 365, 497. ^{1}H NMR (400 MHz, DMSO-d_6): δ = 8.48 (s, 1H, C*H*=N), 7.97 (t, 1H, Py-H_4), 7.70 (d, 1H, Py-H_3). 7.22 (d, 2H, *o*-Ph), 6.89 (d, 1H, Py-H_5), 6.63 (d, 2H, *m*-Ph), 5.44 (s, 2H, NH_2) 3.96 (s, 3H, OCH_3). FT-IR (KBr, cm^{-1}): 3437 (w, ν_{N-H}), 1629 (s, $\nu_{C=N}$), 1594 (s), 1479 (s), 1434 (m), 1309 (m), 1094 (s), 1009 (m), 958 (m), 800 (m), 624 (m), 585 (w). Element analysis for $C_{15}H_{16}C_{l2}N_3OCdCl_2$ (M_r: 412.59): Calcd: C, 37.84%; H, 3.18%; N, 10.18%. Found: C, 37.35%; H, 3.58%; N, 10.67%.

$C_{15}H_{19}N_3OHgCl_2$, Yield: 78%, UV-vis (nm, in ethanol, 25 ºC): 207, 244, 307, 367. ^{1}H NMR (400 MHz, DMSO-d_6): δ = 8.79 (s, 1H, C*H*=N), 8.05 (t, 1H, Py-H_4), 7.73 (d, 1H, Py-H_3). 7.33 (d, 2H, *o*-Ph), 7.16 (d, 1H, Py-H_5), 6.63 (d, 2H, *m*-Ph), 5.64 (s, 2H, NH_2), 4.01 (s, 3H, OCH_3). FT-IR (KBr, cm^{-1}): 3445 (b, ν_{N-H}), 1627 (s, $\nu_{C=N}$), 1596 (s), 1554 (s), 1515 (m), 1475 (s), 1293 (s), 1172 (s), 1098 (m), 957 (w), 838 (m), 793 (m), 584 (m). Element analysis for $C_{15}H_{16}C_{l2}N_3OHgCl_2$ (M_r: 500.76): Calcd: C, 31.18%; H, 2.62%; N, 8.39%.

Found: C, 31.35%; H, 2.78%; N, 8.29%.

2.2 Assembly of DSSCs

The FTO conducting glass (Fluorine-doped SnO_2, sheet resistance 15 Ω per square, transmission 90% in the visible) was purchased from NSG, Japan, and cleaned by a standard procedure. N719 [cis-bis(isothiocyanato)bis(2,2-bipyridyl-4,4-dicarboxylato)-ruthenium(II)bis-tetrabutylammonium] was purchased from Solaronix Company, Switzerland. Dye-sensitized solar cells were fabricated using the following procedure. The TiO_2 paste was cast onto the FTO substrate by the screen-printing method, followed by drying at 100 ºC for 5 min and this process was repeated for six times, then followed by sintering at 500 ºC for 15 min in air to obtain a transparent TiO_2 photoelectrode with the thickness of ca. 10 μm. The co-sensitized electrodes were prepared by immersing the obtained mesoporous TiO_2 photoelectrode into 0.3 mM ZnL, CdL or HgL solution in absolute ethanol for 2 h and washed with ethanol and dried with blower, then further immersing the electrodes in 0.3 mM N719 solution in absolute ethanol for 12 h, and then washed with ethanol and dried with blower again. The single N719 sensitized electrodes were prepared by only immersing TiO_2 photoelectrode into 0.3 mM N719 solution in absolute ethanol for 14 h. The electrolyte used in this work was 0.5 M LiI + 0.05 M I_2 + 0.1 M tert-butyl pyridine in a 1:1 (volume ratio) of acetonitrile-propylene carbonate. The platinum counter electrode was prepared by depositing H_2PtCl_6 paste onto the FTO glass substrates and then sintered at 450 ºC for 30 min. The cells were assembled by sandwiching the electrolyte between the dye sensitized photoanode and the counter electrode and assembly was held together using mini-binder clips.

2.3 Instrumentation and measurements

UV-visible absorption spectra in ethanol solution were recorded on a model SPECORD S600 UV-visible spectrophotometer (Germany Jena), and absorption spectra of TiO_2 films were recorded on a model UV-2250 spectrophotometer (Japan Shimadzu). Fluorescence properties of the synthesized complexes were obtained using an FLS920 spectrometer (Edinburgh) equipped with a peltier-cooled R928 photomultiplayer tube (Hamamatsu). A Xe900 450 W Xenon arc lamp was used as exciting light source. The cyclic voltammetry (CV) were

measured with a electrochemical workstation (CHI660d, Chenhua, Shanghai) using a three-electrode cell with a Pt working electrode, a Pt wire auxiliary electrode, and a saturated calomel reference electrode in saturated KCl solution. The supporting electrolyte was 0.1 M tetrabutylammonium hexafluorophosphate ($TBAPF_6$, Fluka, electrochemical grade) in ethanol as the solvent. Photocurrent-photovoltage (*I-V*) curves were recorded by Keithley model 2400 digital source meter using a mask with an aperture area of 0.16 cm^{-2}. The irradiance of AM1.5 global sunlight from a filtered 500 W xenon lamp light source was set at 100 mW cm^{-2} and was calibrated by a standard silicon solar cell (NO. NIMMS1123, calibrated by National Institute of Metrology, P. R. China). Based on *I-V* curve, the fill factor (*FF*) is defined as: $FF = (J_{max} \times V_{max})/(J_{sc} \times V_{oc})$, where J_{max} and V_{max} are the photocurrent density and photovoltage for maximum power output; J_{sc} and V_{oc} are the short-circuit photocurrent density and open-circuit photovoltage, respectively. The overall energy conversion efficiency η is defined as: $\eta = (FF \times J_{sc} \times V_{oc})/P_{in}$ where P_{in} is the power of the incident light. Monochromatic incident photon-to-electron conversion efficiency (IPCE) were measured on an EQE/IPCE spectral response system (Newport). The surface photovoltage spectrum (SPS) instrument was assembled by Jilin University, in which monochromatic light was obtained by passing light from a 500W xenon lamp through a double-prism monochromator (SBP300, China), and the signal were collected by a lock-in amplifier (SR830, Stanford). Electrochemical impedance spectroscopy (EIS) were recorded by CHI660D Electrochemical Analyzer (Chenhua, China), and the measurements were taken over a frequency range of 0.1-100 kHz under standard global AM1.5 solar irradiation or in the dark by applying a forward bias of -0.75V. 1H NMR (400 MHz) spectra were recorded on a Bruker Avance-400 spectrometer using $Si(CH_3)_4$ as an internal standard at room temperature. Infrared spectra (IR) were obtained from KBr pellets on a Nicolet Avatar-360 Ingrared spectrometer in the 4000-100cm^{-1} region. Elemental analyses were performed on a Perkin-Elmer 2400 element analyzer. The single-crystal X-ray diffraction data for ML were collected on a Rigaku R-AXIS RAPID IP diffractometer equipped with graphite-monochromated Mo KR radiation (λ = 0.71073 Å), operating at 293 ± 2 K. The structures were solved by direct methods and refined by full-matrix least-squares based on F^2 using the SHELXTL 5.1 software package (Sheldrick G M. SHELXTL NT Crystal Structure Analysis Package [CP]. version 5.10; Bruker AXS, Analytical X-ray System: Madison, WI,

1999). The hydrogen atoms residing on the carbon atoms were located geometrically. All non-hydrogen atoms were refined anisotropically.

3. Results and discussions

3.1 Synthesis and structures of ZnL, CdL and HgL

The synthetic routes and molecular structures of ZnL, CdL and HgL are depicted in Scheme 1. All of the three complexes were obtained in good yields (*ca.* 75-78%) as air stable yellowish solids. And all the complexes were characterized by ^{1}HNMR, UV-vis, and IR spectroscopy as well as element analysis. Molecular structures of ZnL and HgL were further determined by single-crystal X-ray diffraction analysis, but a suitable single crystal of CdL was not obtained. Crystal structure data and details of data collection together with the structure refinement are given in Table 1. Selected bond lengths and angles of complexes ZnL and HgL are listed in Table 2. Hydrogen bonding data of complexes ZnL and HgL are listed in Table 3.

The X-ray structural analysis of the single-crystals reveals that ZnL and HgL are isostructural. Single crystal X-ray diffraction analysis also reveals that the complexes of ZnL and HgL crystallize in the triclinic system, $P\bar{1}$ space group. The complex of ML (M=Zn, Hg) has 20 non-hydrogen atoms in the asymmetric unit, which contain one M^{2+} cation, one ligand (N-((6-methoxylpyridin-2-yl)methylene)-*p*-phenylenediimine, half-hydrolyzed from N,N'-bis((6-methoxylpyridin-2-yl)methylene)-*p*-phenylenediimine) and one acetonitrile molecule with all in general positions (Fig. 1). Center metal M^{2+} is four-coordinated: one pyridine N atom, one imino N atom and two chlorine atoms, and displays a slightly distorted tetrahedron arrangement (Fig. 1). For ZnL, the bond angles of N-Zn-N and Cl-Zn-Cl are 81.39(15)° and 113.43(6)°, respectively; the dihedral angle of benzene ring and pyridine ring is 5.77°, which is almost coplanar due to coordinating with Zn^{2+}; the Zn-N bond has a average bond length of 2.074 Å and the imino C=N bond has typical double-bond characteristics, with bond length of 1.287(6) Å. For HgL, the bond angles of N-Hg-N and Cl-Hg-Cl are 73.00(30)° and 111.06(12)°, respectively; the dihedral angle is 4.11°; the average Hg-N bond length is 2.323 Å and the imino C=N bond with bond length of 1.265(12) Å also has typical double-bond characteristics.

A 3-D supramolecular structure of HgL is obtained by π–π stacking interactions (π–π

stacking interactions of 3.5 Å) and hydrogen bonding interactions (see Fig. 2). As for ZnL, it is similar to HgL.

Table 1 Crystal data and crystal refinement for ZnL and HgL

Data		ZnL	HgL
Formula		$C_{15}H_{19}N_3OZnCl_2$	$C_{15}H_{19}N_3OHgCl_2$
Formula weight		365.56	500.76
Crystal system		Triclinic	Triclinic
Space group		$P\bar{1}$	$P\bar{1}$
Unit cell dimensions	a/Å	7.5850(15)	7.5770(15)
	b/Å	9.3580(19)	9.3950(19)
	c/Å	13.408(3)	13.630(3)
	α/°	99.77(3)	99.83(3)
	β/°	94.79(3)	95.31(3)
	γ/°	108.62(3)	108.01(3)
Volume ($Å^3$)		879.1(3)	898.2(3)
Z		2	2
D_{calcd}, g m^{-3}		1.528	1.996
μ, mm^{-1}		1.708	8.873
θ range (°)		3.03° to 27.48°	3.03° to 27.48°
Limiting indices		$-8\le h\le 9$ $-12\le k\le 12$ $-17\le l\le 17$	$-9\le h\le 9$ $-12\le k\le 12$ $-17\le l\le 17$
Data/restraints/parameters		3967 / 0 / 209	4072 / 0 / 209
GOF on F^2		0.941	0.963
Final R indices [I > 2σ(I)]	R_1[a]	0.0515	0.0505
	wR_2[b]	0.1399	0.1367
R indices (all data)	R_1[a]	0.0970	0.0866
	wR_2[b]	0.1725	0.1666
Largest diff. peak/hole ($e·Å^{-3}$)		0.365/ – 0.484	0.910/ – 1.548

[a] $R1 = \Sigma||Fo| - |Fc||/\Sigma|Fo|$.
[b] $wR2 = [\Sigma[w\,(Fo^2 - Fc^2)^2]/\Sigma[\,w\,(Fo^2)^2]]^{1/2}$.

Table 2 Selected bond lengths (Å) and angles (deg) for ZnL and HgL

	ZnL(M=Zn)	HgL(M=Hg)
M(1)-N(1)	2.063(4)	2.288(8)
M(1)-N(2)	2.086(4)	2.358(7)
M(1)-Cl(1)	2.206(2)	2.377(3)
M(1)-Cl(2)	2.244(2)	2.467(3)
N(2)-C(6)	1.287(6)	1.265(12)
N(1)-M(1)-N(2)	81.39(15)	73.00(30)
N(1)-M(1)-Cl(1)	119.62(11)	126.80(20)
N(2)-M(1)-Cl(1)	116.74(11)	123.50(20)
N(1)-M(1)-Cl(2)	113.73(11)	112.65(19)
N(2)-M(1)-Cl(2)	107.58(10)	103.30(20)
Cl(1)-M(1)-Cl(2)	113.43(6)	111.06(12)

Table 3 Hydrogen-bond (Å, deg) for ZnL and HgL

D-H···A	d(H..A)	<DHA	d(D..A)
ZnL			
N3-H3A···N4 [-x, -y+1, -z]	2.331	165.56	3.172
N3-H3B···Cl2 [-x, -y, -z+1]	2.549	166.01	3.389
HgL			
N3-H3A···Cl2 [-x, -y-1, -z+1]	2.601	160.79	3.425
N3-H3B···N4 [-x, -y, -z+1]	2.294	170.51	3.146

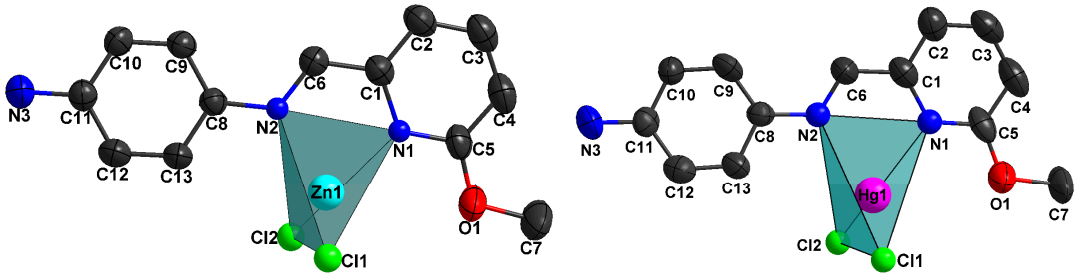

Fig. 1 Molecular structural unit of ZnL and HgL (hydrogen atoms and free acetonitrile molecule are omitted for clarity).

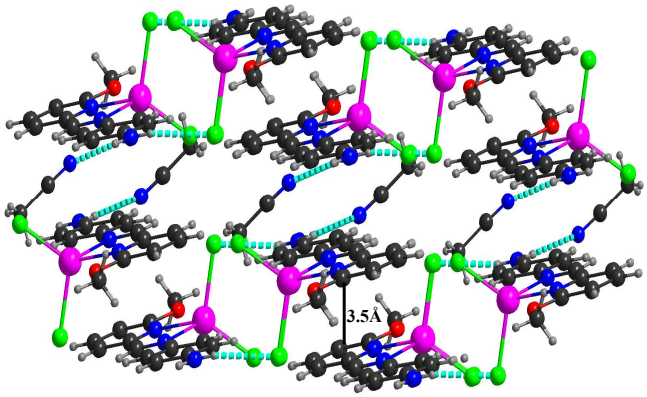

Fig. 2 Packing diagram of complex HgL. Hydrogen bonds are indicated by dashed lines.

3.2 Optical properties of ZnL, CdL and HgL

The absorption spectra of the prepared complexes and N719 in ethanol solutions are shown in Fig. 3, and the corresponding data are listed in Table 4. In the UV-vis spectra, the complexes of ZnL, CdL and HgL exhibit two major prominent bands. The first one at *ca.* 280-325 nm is attributed to localized aromatic π-π* transitions, and the other one at *ca.* 325-700 nm, 325-675nm and 325-525 nm for ZnL, CdL and HgL, respectively, is attributed to intramolecular charge transfer (ICT) absorption. Compared with the absorption spectra of

N719, apparently, the absorption spectra of ZnL, CdL and HgL could compensate for that of N719 in the low wavelength region of visible spectrum.

As shown in Table 4, the ICT absorption (λ_{max}) appears at 365 nm for ZnL and CdL, and 367 nm for HgL. The molar extinction coefficients in the visible region are 32,571 M^{-1} cm^{-1} for ZnL, 29,860 M^{-1} cm^{-1} for CdL and 28,353 M^{-1} cm^{-1} for HgL. All of these are much higher than that of the ruthenium complex N719.[29] A higher molar extinction coefficient around 365-367 nm indicates that the ZnL, CdL, and HgL possess a higher light harvesting ability in this wavelength region compared with N719 and I_3^- (25,000M^{-1} cm^{-1}).[30] Hence it can be predicted that the photon lost due to the light absorption by I_3^- will be suppressed by the use of ZnL, CdL or HgL as a co-sensitizer and co-adsorbent due to the competition between ZnL, CdL or HgL and I_3^- to absorb light.

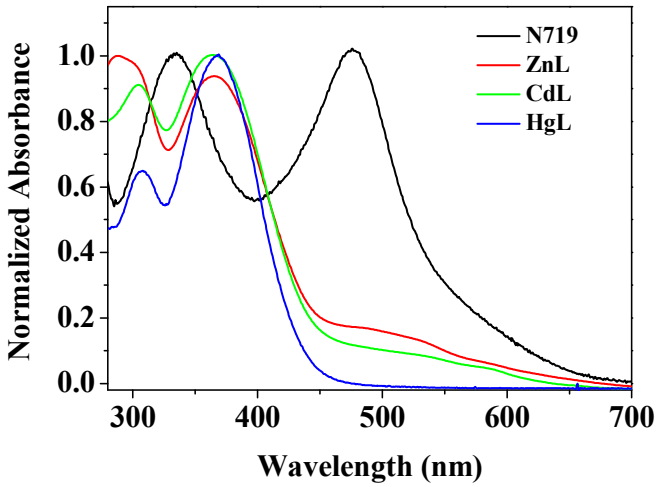

Fig. 3 UV-visible absorption spectra of ZnL, CdL, HgL and N719 in ethanol.

The absorption spectra of ZnL/N719, CdL/N719 and HgL/N719 co-sensitized TiO_2 films are shown in Fig. 4. As shown in Fig. 4, the absorption of N719 on TiO_2 film in visible light region is remarkably broadened and its peak at 475 nm in ethanol solutions is red-shifted to 555 nm. This could be ascribed to the aggregation[31] or electronic coupling of the dyes on the TiO_2 surface.[32] The interaction between the carboxyl group and the surface Ti^{4+} ions may lead to increased delocalization of the π^* orbital of the conjugated framework. The energy of the π^* level is decreased by this delocalization, resulting in the red shift for the absorption spectra.

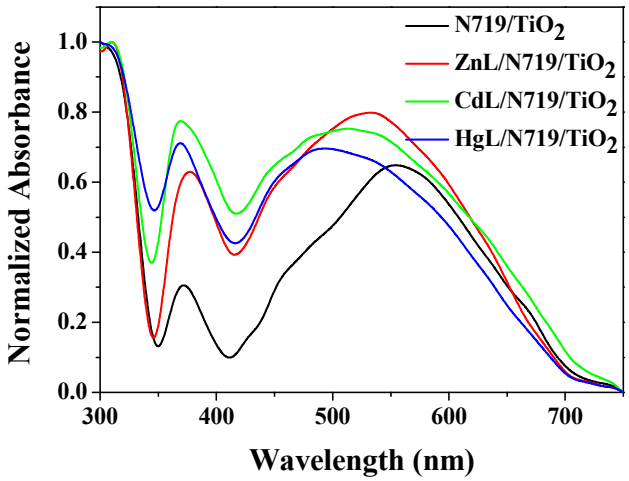

Fig. 4 UV-visible absorption spectra of ZnL, CdL, HgL and N719 on TiO_2 films.

Table 4 Experimental data for spectral and electrochemical properties of the synthesized complexes

Dyes	λ_{abs}(nm)[a]	$\varepsilon(M^{-1}cm^{-1})$[a]	λ_{em}(nm)[a,b]	$E_{0\text{-}0}$(eV)[c]	E_{HOMO}(eV)[d]	E_{LUMO}(eV)[d]
ZnL	365	32571	481	2.90	-5.09	-2.19
CdL	365	29860	481	2.89	-5.01	-2.12
HgL	367	28353	477	2.92	-5.06	-2.14

[a] Absorption and emission spectra were recorded in ethanol solution (3×10^{-4} M) at room temperature.
[b] Complexes were excited at their absorption maximum value
[c] Optical band gap calculated from intersection between the absorption and emission spectra.
[d] The values of E_{HOMO} and E_{LUMO} were calculated with the following formula:
HOMO (eV) = -e(E^{ox}_{onset}V + 4.4V); LUMO (eV) = $E_{HOMO} + E_{0\text{-}0}$
where $E_{0\text{-}0}$ is the intersection of absorption and emission of the complexes.

In comparison of the absorption of N719 on TiO_2 film, the absorption peaks for ZnL/N719, CdL/N719 and HgL/N719 on the TiO_2 film are blue-shifted by 23, 43 and 62 nm, respectively, displaying the bands at 532, 512 and 493 nm. This indicated that when ZnL, CdL or HgL is used as co-sensitizer and co-adsorbent, the aggregation of N719 is alleviated and the new interactions between dye-dye and dye-TiO_2 are introduced, leading to the absorption of N719 on TiO_2 film blue-shifted. Furthermore, the absorption of co-sensitized film is enhanced remarkably when ZnL, CdL or HgL was introduced, especially in the region of 320-550nm. This is consistent with the result that the absorption spectra of ZnL, CdL and HgL could compensate for that of N719 in the low wavelength region of the visible spectrum based on the spectra shown in Fig. 3.

The emission spectra of ZnL, CdL and HgL are illustrated in Fig. 5. All of them exhibit strong luminescence in the region of wavelength 350-750 nm, and it is worth to note that all of the emission spectra of ZnL, CdL and HgL overlap with the excitation spectra of N719

inordinately. This indicates that N719 could synchronously accept the energy from the incident light and the excited ML, which will broaden the spectra response of N719 in the region of 350-750 nm.

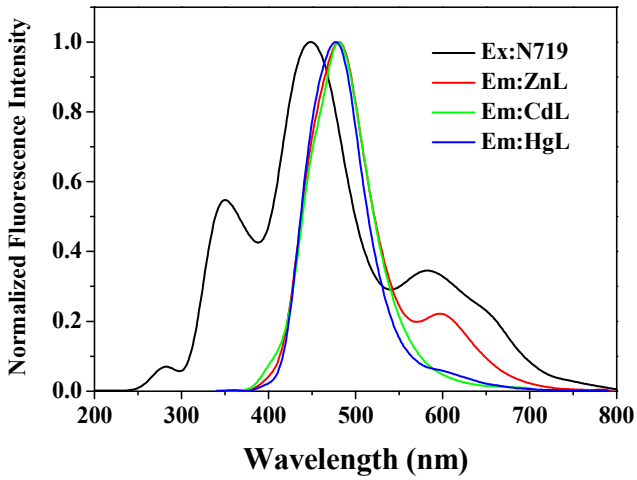

Fig. 5 The emission spectra of dyes in ethanol solution.

3.3 Electrochemical properties of ZnL, CdL and HgL

Energy-level matching is crucial in selecting sensitizer. In order to estimate the HOMO and LUMO energy levels of ZnL, CdL and HgL, cyclic voltammetry (CV) was carried out in a three-electrode cell and an electrochemistry workstation. The experimental data for electrochemical properties of ML are summarized in Table 4. As estimated from the intersection of the absorption and emission spectra, the excitation transition energy ($E_{0\text{-}0}$) of ZnL, CdL and HgL are 2.90, 2.89 and 2.92 eV, respectively. Consequently, the HOMO values of ZnL, CdL and HgL are caculated based on their first redox potentials as -5.09, -5.01 and -5.06 eV, respectively, and the LUMO levels of ZnL, CdL and HgL calculated from E_{HOMO} + $E_{0\text{-}0}$, are -2.19, -2.12 and -2.14 eV, respectively.[33] The HOMO and LUMO energy levels of ZnL, CdL and HgL are shown in Scheme 2. It shows that the energy levels of ZnL, CdL and HgL are appropriate for the DSSCs system containing TiO_2. The LUMO levels lied above the conduction band (CB) of the TiO_2 semiconductor (-4.40 eV vs vacuum), indicating efficient electron injection, and the HOMO energy levels lied below the I^-/I_3^- redox electrolyte (-4.60 eV vs vacuum) which is further improved negatively about 0.3 V by adding additives such as 4-tert-butyl pyridine (TBP) to the I^-/I_3^- redox electrolyte,[34] providing sufficient driving force for dye regeneration.[35]

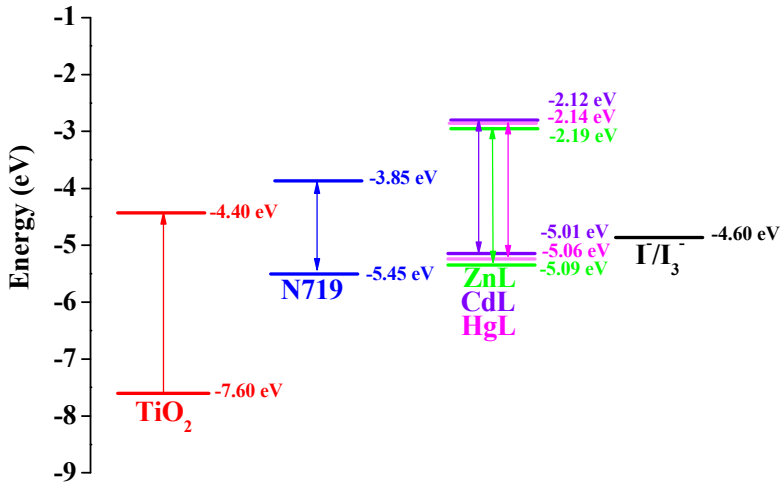

Scheme 2 Schematic energy diagram of HOMO and LUMO for dyes compared to the energy levels calculated for TiO_2.

3.4 Photovoltage properties of DSSCs

ZnL, CdL and HgL were employed as co-sensitizers and co-adsorbents to fabricate ML/N719 photoanodes. The current-voltage (*J-V*) characteristic of the DSSCs devices based on N719, ZnL/N719, CdL/N719 and HgL/N719 photoanodes are shown in Fig.6, and the corresponding cells performance are summarized in Table 5. Upon co-sensitization, the performances of cells are all improved. The values of J_{sc}, V_{oc} and η are improved in the order of ZnL/N719 > CdL/N719 > HgL/N719, respectively. The ZnL/N719 device yield a J_{sc} of 14.46 mA cm^{-2}, a V_{oc} of 0.74 V, a fill factor (*FF*) of 0.62 and η of 6.65%. All the parameters are significantly higher than that of the device only sensitized by N719.

Table 5 *J-V* performance of DSSCs based on different photoelectrodes

Photoelectrode	J_{sc}/mA/cm^2	V_{oc}/V	*FF*	η/%
N719/TiO_2	12.36	0.68	0.62	5.22
ZnL/N719/TiO_2	14.46	0.74	0.62	6.65
CdL/N719/TiO_2	14.35	0.73	0.60	6.30
HgL/N719/TiO_2	13.92	0.70	0.61	5.96

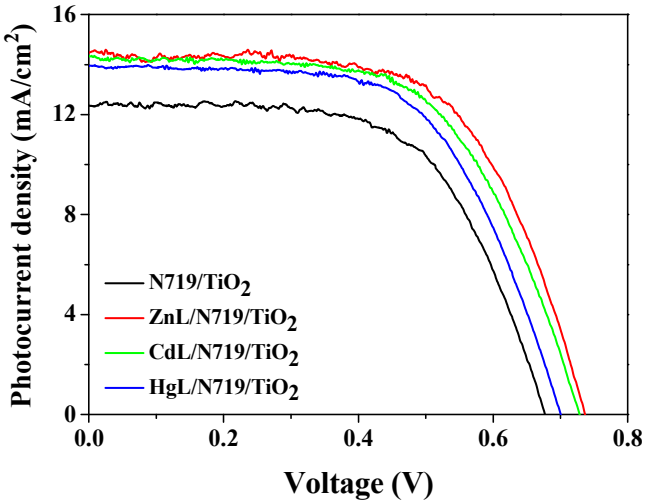

Fig. 6 *J-V* curves for DSSCs based on co-sensitized photoelectrodes and N719 sensitized photoelectrode under irradiation.

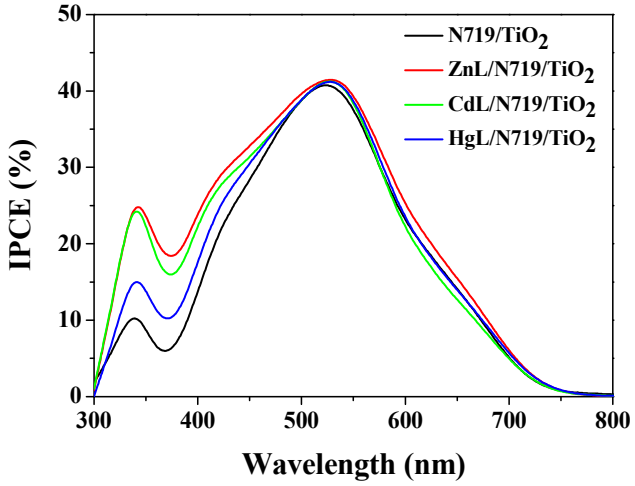

Fig. 7 IPCE spectra of DSSCs based on single N719 sensitized and co-sensitized photoelectrodes.

The IPCE spectra were collected in order to interpret the enhancement of J_{sc} (Fig. 7). The DSSCs containing only N719 dye has a broad IPCE spectrum from 300-750 nm but a decrease in the wavelength range of 340-450 nm, which is due to the competitive light absorption between I_3^- and N719. When ML is used as co-sensitizer and co-adsorbent, this decrease are restored in the order of ZnL/N719 > CdL/N719 > HgL/N719, which is attributed to the fact that the ML complexes have attached to the TiO_2 surface effectively and contributed to the electron injection into the conduction band of the TiO_2. This means the co-sensitization of N719 and ML has a significant synergy and compensatory effect on light

harvesting and electron collection on TiO_2. Based on the IPCE and the absorption spectra, the cell's higher J_{sc} in the case of co-sensitization is ascribed to better light harvesting in the low wavelength region, where the absorption of N719 is compensated and the competitive light absorption of I_3^- is overcome.

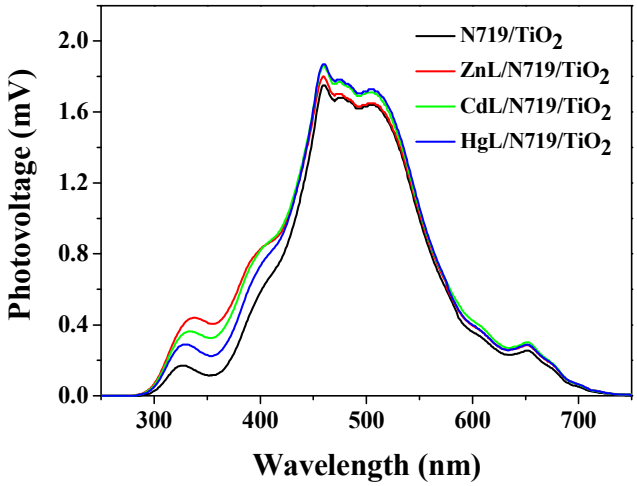

Fig. 8 SPS of DSSCs based on different photoelectrodes.

To further investigate the enhanced performance of DSSCs, the surface photovoltages of DSSCs based on different photoelectrodes were investigated, which is a well-established contactless technique for surface state distribution[36,37] The curves in Fig. 8 indicate that co-sensitization could result in stronger photovoltage signals between 300 and 750 nm, especially in the region of 300-450 nm. The photovoltage signals increased in the order of ZnL/N719 > CdL/N719 > HgL/N719, which indicates that the separation efficiency of electrons and holes correlate strongly with ZnL, CdL and HgL, and the enhancement of the photovoltage signals in the region of 300-450 nm is attributed to the overcoming of the competitive light absorption of I_3^- and compensation of N719 absorption; besides, the enhancement of the photovoltage signals in the region of 300-700 nm may also could be attributed to the reduction of N719 aggregation and interaction of ML and N719, which further support the results from IPCE.

The dark current-voltage characteristics of the DSSCs based on the ML/N719 and N719 dyes are shown in Fig. 9, which indicates the recombination of injected electron with I_3^-. It shows that the dark current is lower for the co-sensitized system compared with that of

single N719 sensitized DSSC, which is in the order of ZnL/N719 < CdL/N719 < HgL/N719. This could be explained as follows: as shown in absorption spectra, co-sensitization of N719 with ML on TiO_2 film produces a blue shift, indicating that the N719 molecules orientate themselves in a more parallel conformation, leaving space for the ML co-sensitizer. The interaction from each other forms a dense packing of dyes on TiO_2 electrode or an insulating layer composed of ML and N719, which could effectively suppress charge recombination and thereby enhance V_{oc}. It is noticed that the V_{oc} value is in the opposite order with the dark current, that is ZnL/N719>CdL/N719>HgL/N719>N719. When ML was used as co-sensitizers and co-adsorbents, the J_{sc} and V_{oc} were all enhanced, both of which lead to the improvement of η. The improved J_{sc} and V_{oc} with unpronounced difference in FF, make it obtained higher η, which is in the same order with J_{sc} and V_{oc}.

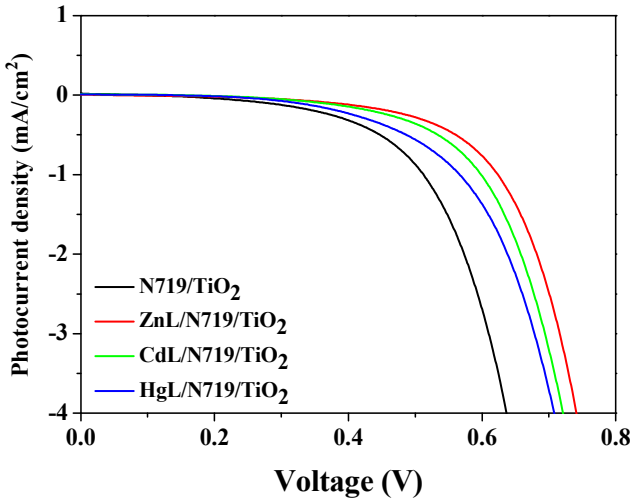

Fig. 9 *J-V* curves for DSSCs based on co-sensitized photoelectrodes and N719 sensitized photoelectrode in dark.

When the crystal structures of the complexes are taken into account, it is found that the enhancement of co-sensitized DSSCs performance compared with that of single N719 sensitized DSSCs may be due to the key structural feature of complex. In the complex, the center metal is chelating with two N electron donors of the ligand and forming a five membered ring which is adjacent to the pyridine ring. The five membered ring, pyridine ring and benzene ring are almost coplanar, thereby, the rigidity to the molecular structure is increased. The well co-planarity and rigidity mean easier electron transfer and are in favor of

electrochemical property. Furthermore, the complexes ML extend as supermolecules through hydrogen bonding and π-π interactions, which make the electron-donating ability of ML better when they are used in DSSCs as co-sensitizer. All of these structural features of ML result in obtaining higher performance of co-sensitized cells than that of cells sensitized by single N719. Meanwhile, it is noted that the DSSC performance is gradually enhanced in the order of HgL < CdL < ZnL. To some extent, this difference observed in the DSSC performance likely has their origins including the metal ion in the unit cell and the steric proximity of ligand L. For HgL, the larger atom radius of Hg likely increase Hg-N average bond length, which is 2.323 Å (the average Zn-N bond length is 2.074 Å), and the narrow angle formed by the chelating L in HgL, N1-Hg-N2 is 73.00°, which is significantly smaller than that in ZnL (the bond angle of N1-Zn-N2 is 81.39°). In this case, the distance between M to electron donating group N is increased. Also, it is worthwhile to note that the distance between benzene ring and five member ring including M is increased, from ZnL to HgL, namely, the bond length C8-N2 is 1.41 Å in HgL, which is longer than the corresponding value in ZnL (the bond length C8-N2 is 1.40 Å in ZnL).This is probably caused by the steric hindrance. Apparently, the increased distance is not good for electron transfer. Therefore, the performance of co-sensitized cell is in the order of ZnL/N719 > CdL/N719 > HgL/N719.

3.5 Electrochemical impedance spectroscopy studies of DSSCs

EIS is a powerful technique for the analysis of interfacial electronic and ionic transport processes in an electrochemical device.[38,39] It is a steady state method to measure current response based on application of an ac voltage at different frequencies. Herein, we utilized EIS to analyze charge carrier dynamics in the interfacial regions of solid-liquid layers. The Nyquist plots of EIS for DSSCs based on different photoelectrodes measured under standard global AM1.5 solar irradiation and in the dark by applying a forward bias of -0.75V are illustrated in Fig. 10. Only two semicircles were observed for DSSCs in our experiments, which is different from what is reported in the literature that three semicircles should be observed in the frequency range of 0.1 to 10 kHz in the Nyquist plots. This can be explained as the conventional diffusion resistance of the redox couple is greatly overlapped by the charge transfer resistance due to the short diffusion length of I^- ion available with the thin spacer and the low viscosity of the solvents used in the electrolyte.

Under light illumination, EIS was utilized to analyze the charge transport resistance at the TiO_2/dye/electrolyte interface for its significance on the efficiency of DSSCs.[40-42] As shown in Fig. 10a, the two semicircles located in high and middle frequency regions (left to right) are attributed to the electrochemical reaction at the Pt/electrolyte interface and the charge transfer at the TiO_2/dye/electrolyte interface.[43-45] The radius of the large semicircle located in middle frequency regions in the Nyquist plots decrease after co-sensitized with ML, and the values are in the order of ZnL/N719 < CdL/N719 < HgL/N719 < N719, which indicates a decrease of the electron transfer impedance (R_{ct}) and a increase of charge transfer rate at this interface after co-sensitization.

In dark conditions, as shown in Fig. 10b, the two semicircles located in high, middle and low frequency regions (left to right) of Nyquist plots are attributed to the redox reaction at the Pt counter electrode and the electron transfer at the TiO_2/dye/electrolyte interface.[43-46] Therefore the larger semicircle observed in middle frequency region represents the resistances of the charge transfer from the TiO_2 to the electrolyte (back recombination resistance R_{rec}). The radius of this semicircle increase after co-sensitized with ML, indicating an increase of R_{rec}. A large R_{rec} means the small charge recombination rate and vice versa. The radius of the semicircle observed in middle frequency range lies in the order of ZnL/N719 > CdL/N719 > HgL/N719 > N719, indicating sequence of R_{rec} at the TiO_2/dye/electrolyte interface. The increased value of R_{rec} for DSSCs implies the retardation of the charge recombination between injected electron and I^-_3 ions in the electrolyte, with a consequent increase of V_{oc}. This appears to be consistent with the larger V_{oc} values sequence.

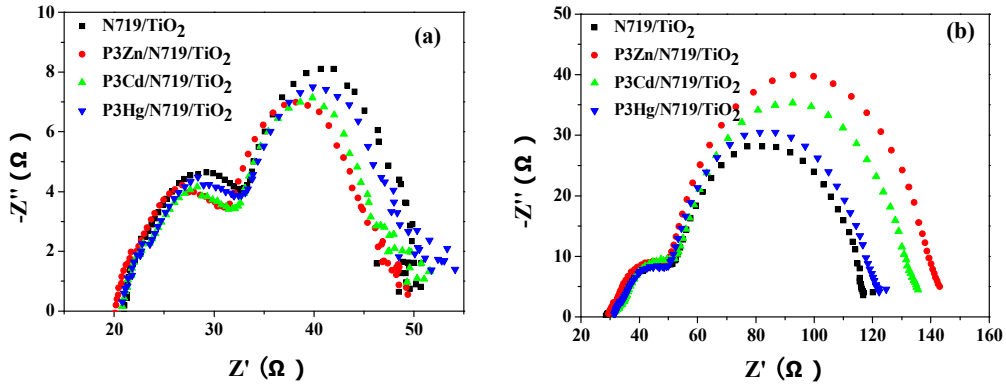

Fig. 10. Nyquist plots of EIS for DSSCs based on different photoelectrodes measured under standard AM1.5 G solar irradiation (a) or in dark (b) at forward bias -0.75V.

Table 6 Parameters obtained by fitting the impedance spectra of solar cells

DSSCs	R_{ct}/ Ω	R_{rec}/ Ω
N719	13.60	68.30
ZnL/N719	13.02	83.50
CdL/N719	13.07	76.64
HgL/N719	13.11	73.07

Also, a suggested impedance model by Bisquert is used to fit curves in middle frequency region of Nyquist plots using Z-view software.[38] R_{ct} and R_{rec} at the TiO_2 surface were deduced by this method and are list in Table 6. The values of R_{ct} are in the order of ZnL/N719 < CdL/N719 < HgL/N719 < N719 and R_{rec} are in the order of ZnL/N719 > CdL/N719 > HgL/N719 > N719. These again confirm the analysis above that after co-sensitization with ML, the charge transfer rate increased and the charge recombination rate decreased, both of which are favorable to enhance the performance of DSSCs.

According to the EIS analysis, the charge recombination resistance is larger and the charge transport resistance is smaller for the DSSCs based on ML/N719 than that for the DSSCs based on N719, indicating that co-sensitization has effectively modified the TiO_2/dye/electrolyte interface and increased the J_{sc} and the V_{oc}. In the co-sensitized system, a better dye coverage helps to passivate the TiO_2 surface or form an insulating molecular layer composed of ML and N719 molecules and thus reduces the recombination due to electron back-transfer between TiO_2 and I_3^-, which ultimately increases the V_{oc} compared with those of individual sensitized devices.

4. Conclusions

In conclusion, the new synthesized d^{10} coordinate complexes based on N,N'-bis((6-methoxylpyridin-2-yl)methylene)-*p*-phenylenediimine ligand have a significant effect on the performance of DSSCs when they were used as co-sensitizers and co-adsorbents, it could improve both J_{sc} and V_{oc}. The co-sensitized devices exhibit enhanced performance in the order of ZnL/N719 > CdL/N719 > HgL/N719, and all of them are higher than that of single N719 sensitized solar cells. The ZnL/N719 co-sensitized device yields the best overall efficiency of 6.65%, which is greater than that of the device containing only N719 (5.22%). J_{sc} is enhanced because of the combined light harvesting of N719 and synthesized complex with complementary absorption spectra, reduction of dye aggregation,

offsetting of the competitive light absorption of I^-/I_3^- and favorable energy alignments, while V_{oc} is enhanced because of the retarded charge recombination due to a better dye coverage on the TiO_2 surface or formation of an insulating molecular layer composed of ML and N719 molecular which suppress the recombination of the injected electron with I_3^- ions.

Moreover, these devices are made without scattering layers, $TiCl_4$ treatment, or antireflecting coatings, but with less internal area than fully optimized TiO_2 electrodes and the performance is competitive with solar cells made with single ruthenium complex N719, reaching up to 6.65% under similar conditions. The high efficiency and simple fabrication suggests very bright application prospects of this method in large-scale production of DSSCs.

Acknowledgements

This work was supported by National Natural Science Foundation of China (Grant Nos. 21171044 and 21371040), National key Basic Research Program of China (973 Program, No. 2013CB632900) and Program for Innovation Research of Science in Harbin Institute of Technology.

Notes and references

1 B. O'Regan and M.Grätzel, *Nature*, 1991, **353**, 737–740.

2 M. K. Nazeeruddin, F. D. Angelis, S. Fantacci, A. Selloni, G. Viscardi, P. Liska, S. Ito, B. Takeru and M. Grätzel, *J. Am. Chem. Soc.*, 2005, **127**, 16835–16847.

3 M. Grätzel, *J. Photochem. Photobiol. C*, 2003, **4**, 145–153.

4 A. Yella, H. W. Lee, H. N.Tsao, C. Yi, A. K. Chandiran, M. K. Nazeeruddin, E. W. G. Diau, C. Y.Yeh, S. M. Zakeeruddin and M. Grätzel, *Science*, 2011, **334**, 629–634.

5 J. J. Cid, J. H. Yum, S. R. Jang, M. K. Nazeeruddin, E. M. Ferrero, E. Palomares, J. J. Ko, M. Grätzel and T. Torres, *Angew. Chem., Int. Ed.*, 2007, **46**, 8358–8362.

6 J. H. Yum, S. R. Jang, P. Walter, T. Geiger, S. Nüesch, K. J. Ko, M. Grätzel and M. K. Nazeeruddin, *Chem. Commun.*, 2007, 4680–4682.

7 C. M. Lan, H. P. Wu, T. Y. Pan, C. W. Chang, W. S. Chao, C. T. Chen, C. L. Wang, C. Y. Lin and E. W. G. Diau, *Energy & Environmental Science*, 2012, **5**, 6460–6464.

8 M. Mojiri-Foroushani, H. Dehghani and N. Salehi-Vanani, *Electrochimica Acta*, 2013, **92**, 315–322.

9 R. Y. Ogura, S. Nakane, M. Morooka, M. Orihashi, Y. Suzuki and K. Noda, *Appl. Phys. Lett.*, 2009, **24**, 073308.

10 P.J. Holliman, M. Mohsen, A. Connell, M.L. Davies, K. Al-Salihi, M.B. Pitak, G.J. Tizzard, S.J. Coles, R.W. Harringston, W. Clegg, C. Serpa, O.H. Fontes, C. Charbonneau and M.J. Carnie, *J. Mater. Chem.*, 2012, **22**, 13318–13327.

11 K.M. Lee, Y.C. Hsu, M. Ikegami, T. Miyasaka, K.R.J. Thomas, J.T. Lin and K.C. Ho, *J. Power Sources*, 2011, **196**, 2416–2421.

12 S.Q. Fan, C. Kim, B. Fang, K.X. Liao, G.J. Yang, C.J. Li, J.J. Kim and J. Ko, *J. Phys. Chem. C*, 2011, **115**, 7747–7754.

13 R. Y. Ogura, S. Nakane, M. Morooka, M. Orihashi, Y. Suzuki and K. Noda, *Appl. Phys. Lett.*, 2009, **24**, 073308.

14 L. Han, A. Islam, H. Chen, C. Malapaka, S. Zhang, X. Yang, M. Yanagida and B. Chiranjeevi, *Energy Environ. Sci.*, 2012, **5**, 6057–6060.

15 H. Ozawa, R. Shimizu and H. Arakawa, *RSC Adv.*, 2012, **2**, 3198–3200.

16 R. Y. Y. Lin, Y. S. Yen, Y. T. Cheng, C. P. Lee, Y. C. Hsu, H. H. Chou, C. Y. Hsu, Y. C. Chen, K. C. Ho, J. T. Lin and C. T. Tsai, *Org. Lett.*, 2012, **14**, 3612–3615.

17 C. Magne, M. Urien and T. Pauporté, *RSC Adv.*, 2013, **3**, 6318–6318.

18 J. Chang, C. P. Lee, D. Kumar, P. W. Chen, L. Y. Lin, K. R. Justin Thomas and K. C. Ho, *J. Power Sources*, 2013, **240**, 779–785.

19 M. K. Wang, N. Chamberland, L. Breau, J. E. Moser, R. Humphry-Baker, B. Marsan, S. M. Zakeeruddin and M. Grätzel, *Nat. Chem.*, 2010, **2**, 385–389.

20 H. N. Tian and L. C. Sun, *J. Mater. Chem.*, 2011, **21**, 10592–10601.

21 B. J. Song , H. M. Song , I. T. Choi, S. K. Kim, K. D. Seo, M. S. Kang, M. J. Lee, D. W. Cho, M. J. Ju and H. K. Kim, *Chem. Eur. J.*, 2011, **17**, 11115–11121.

22 T. Bessho, S. M. Zakeeruddin, C. Y. Yeh, E. W. G. Diau and M. Grätzel, *Angew. Chem. Int. Ed.*, 2010, **49**, 6646–6649.

23 S. Q. Fan, C. Kim, B. Fang, K. X. Liao, G. J. Yang, C. J. Li, J. J. Kim and J. J. Ko, *J. Phys. Chem. C*, 2011, **115**, 7747–7754.

24 H. X. Wang, M. N. Liu, M. Zhang, P. Wang, H. Miura, Y. Cheng and J. Bell, *Phys. Chem. Chem. Phys.*, 2011, **13**, 17359–17366.

25 L. Han, A. Islam, H. Chen, C. Malapaka, S. Zhang, X. Yang, M. Yanagida and B. Chiranjeevi, *Energy Environ. Sci.*, 2012, **5**, 6057–6060.

26 X. Wang, Y. L. Yang, P. Wang, L. Li, R. Q. Fan, W. W. Cao, B. Yang, H. Wang and J. Y. Liu, *Dalton Trans.*, 2012, **41**, 10619–10625.

27 X. Wang, Y. L. Yang, R.Q. Fan and Z. H. Jiang, *New J. Chem.,* 2010, **34**, 2599–2604.

28 L. Y. Zhang, Y. L. Yang, R. Q. Fan, P. Wang and L. Li, *Dyes and Pigments*, 2012, **92**, 1314–1319.

29 D. B. Kunag, S. Ito, B. Wenger, C. Klein, J. E. Moser, R. Humphry-Baker, S. M. Zakeeruddin and M. Grätzel, *J. Am. Chem. Soc.*, 2006, **128**, 4146–4154.

30 G. D. Sharma, S. P Singh, R. Kurchania and R. J. Ball, *RSC Adv.*, 2013, **3**, 6036–6043.

31 G. Janssens, F. Touhari, J. W. Gerritsen, H. V. Kempen, P. Callant, G. Deroover and D.Vandenbroucke, *Chem. Phys. Lett.*, 2001, **344**, 1–6.

32 C. Y. Lin, C. F. Lo, L. Luo, H. P. Lu, C. S. Hung and E. W. G. Diau, *J. Phys. Chem. C*, 2009, **113**, 755–764.

33 C. M. Cardona, W. Li, A. E. Kaifer, D. Stockdale and G. C. Bazan, *Adv. Mater.*, 2011, **23**, 2367–2371.

34 G. Boschloo, L. Ha1ggman and A. Hagfeldt, *J. Phys. Chem. B*, 2006, **110**, 13144–13150.

35 K. R. Justin Thomas, Y. C. Hsu, J. T. Lin, K. M. Lee, K. C. Ho, C. H. Lai, Y. M. Cheng and P. T. Chou, *Chem. Mater.*, 2008, **20**, 1830–1840.

36 H. Irie, Y. Watanabe and K. Hashimoto, *J. Phys. Chem. B*, 2003, **107**, 5483–5486.

37 L. Q. Jing, X. J. Sun, J. Shang, W. M. Cai, Z. L. Xu, Y. G. Du and H. G. Fu, *Sol. Energy Mater. Sol. Cells*, 2003, **79**, 133–151.

38 J. Bisquert, *J. Phys. Chem. B*, 2002, **106**, 325–333.

39 J. Bisquert, A. Zaban, M. Greenshtein and I. Mora-Sero, *J. Am. Chem. Soc*., 2004, **126**, 13550–13559.

40 C. P. Hsu, K. M. Lee, J. T. W. Huang, C. Y. Lin, C. H. Lee, L. P. Wang, S. Y. Tsai and K. C. Ho, *Electrochimica Acta*, 2008, **53**, 7514–22.

41 K. E. Lee, M. A. Gomez, C. Charbonneau and G. P. Demopoulos, *Electrochimica Acta*, 2012, **67**, 208–215.

42 C. Y. Hsu, W. T. Chen, Y. C. Chen, H. Y.Wei, Y. S. Yen, K. C. Huang, K. C. Ho, C. W. Chu and J. T. Lin, *Electrochimica Acta*, 2012, **66**, 210–215.

43 J. Bisquert, *Phys. Chem. Chem. Phys.*, 2003, **5**, 5360–5364.

44 D. Kuang, S. Uchida, R. Humphry-Baker, S. M. Zakeeruddin and M. Grätzel, *Angew. Chem. Int. Ed.*, 2008, **47**, 1923–1926.

45 N. Koide, A. Islam, Y. Chiba and L. Y. Han, *J. Photochem. Photobiol. A Chem.*, 2006, **182**, 296–303.

46 M. K. Nazeeruddin, S. M. Zakeeruddin, R. Humphry-Baker, M. Jirousek, P. Liska, N. Vlachopoulos, V. Shklover, C. H. Fischer and M. Grätzel, *Inorg. Chem.*, 1999, **38**, 6298–6304.

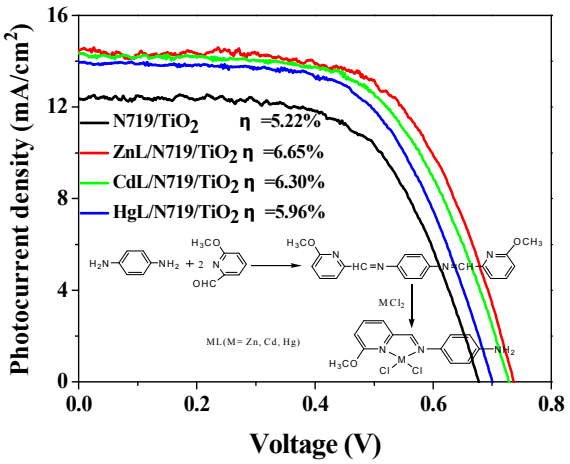

New d^{10} transition metal complexes of ZnL, CdL and HgL enhanced the performance of DSSCs by co-sensitization with N719.